RSC Advances

PAPER

View Article Online
View Journal | View Issue

Cite this: *RSC Adv.*, 2022, **12**, 26815

Synthesis and hybridizing properties of P-stereodefined chimeric [PS]-{DNA:RNA} and [PS]-{DNA:(2′-OMe)-RNA} oligomers†

Katarzyna Jastrzębska, * Anna Maciaszek, Rafał Dolot, Agnieszka Tomaszewska-Antczak, Barbara Mikołajczyk and Piotr Guga

Received 4th August 2022
Accepted 8th September 2022

DOI: 10.1039/d2ra04855h

rsc.li/rsc-advances

Oxathiaphospholane derivatives of 2′-OMe-ribonucleosides and 2′-*O*-TBDMS-ribonucleosides (^{M}N-OTP and ^{T}N-OTP, respectively; nucleobase protected) were synthesized and separated into pure P-diastereomers. X-ray analysis showed the R_P absolute configuration of the phosphorus atom in the *fast*-eluting diastereomer of ^{T}A-OTP. The *fast*- and *slow*-eluting P-diastereomers of ^{M}N-OTP and ^{T}N-OTP were used in the solid-phase synthesis of phosphorothioate dinucleotides (^{M}N$_{PS}$T and N$_{PS}$T, respectively), which were subsequently hydrolyzed with R_P-selective phosphodiesterase svPDE and S_P-selective nuclease P1 to determine the absolute configuration of the phosphorus atoms. P-Stereodefined phosphorothioate ([PS]) 10-mer chimeric oligomers [PS]-{DNA:(2′-OMe)-RNA} and isosequential [PS]-{DNA:RNA} containing two ^{M}N$_{PS}$ or N$_{PS}$ units were synthesized. Melting experiments performed for their complexes with Watson–Crick paired DNA matrix showed that ^{M}N$_{PS}$ or N$_{PS}$ units decrease the thermal stability of the duplexes ($\Delta T_m = -0.5 \div -5.5$ °C per modification) regardless of the absolute configuration of the P-atoms. When the (2′-OMe)-RNA matrix was used an increase in T_m was noted in all cases ($\Delta T_m = +1 \div +7$ °C per modification). The changes in thermal stability of the duplexes formed by [PS]-chimeras with DNA and (2′-OMe)-RNA matrices do not correlate with the absolute configuration of the phosphorus atoms.

Introduction

In the last five decades, many DNA analogs have been chemically synthesized, mainly to improve their stability against nucleases and in this way to ensure long-lasting recognition of the target nucleic acid. This increased stability was expected to produce new probes useful for example for controlling gene expression or biochemical manipulations. To some extent, this goal has been achieved by the introduction of phosphorothioate analogs of DNA ([PS]-DNA),[1] although nonspecific binding to proteins[2] and immunological side effects[3,4] initially hindered their application *in vivo*. [PS]-RNA oligomers were obtained shortly after using phosphoramidite or *H*-phosphonate monomers with sulfurization. Note: interestingly, it has been shown that [PS]-DNA probes in the absence of transfecting agents enter mammalian cells more efficiently than DNA.[5] An explanation based on the dynamic covalent exchange of phosphorothioates with cellular thiols and disulfides has recently been published.[6] Some drugs containing [PS]-DNA and [PS]-RNA-derived units have been approved by the FDA and other agencies, and several others are in advanced clinical trials.[7]

Noteworthy, in 2007 phosphorothioation of DNA was discovered in bacteria,[8] and in 2019, a DNA phosphorothioation-based antiviral system was discovered in archaea.[9] The identified chimeric phosphate:phosphorothioate compounds ([PO]:[PS]) contained the phosphorothioate phosphorus atoms only of R_P absolute configuration.[10] In 2020, the R_P phosphorothioate modification was detected in RNA isolated from prokaryotes and eukaryotes.[11]

Although the phosphorothioate internucleotide bond is isoelectronic with the natural phosphate moiety, the properties of [PS]-DNA differ from natural DNA ([PO]-DNA) in several aspects, mainly due to the different steric requirements of the sulfur atom, the altered affinity for metal ions ("soft" sulfur *vs.* "hard" oxygen), and unsymmetrical distribution of the negative charge in the diester phosphorothioate anion.[12] Depending on the intended application, these altered properties may be considered either disadvantageous or beneficial, but in the vast majority of biology-related experiments, one should consider the stereochemistry of the internucleotide phosphorothioate moieties. Since the substitution of sulfur for a nonbridging oxygen atom creates a stereogenic center, for example, a [PS]-

Centre of Molecular and Macromolecular Studies, Polish Academy of Sciences, Department of Bioorganic Chemistry, Sienkiewicza 112. 90-363 Łódź, Poland. E-mail: kjastrz@cbmm.lodz.pl; Fax: +48-42-6803261; Tel: +48-42-6803248

† Electronic supplementary information (ESI) available: HPLC profiles for the separation of P-diastereomers of **2** and **3**; HR MS, ^{1}H, ^{13}C and ^{31}P NMR spectra for P-diastereomers of **2** and **3**; the crystal data and data collection and refinement parameters for the fast-eluting detritylated **3a** (B′ = Ade^{Bz}); MALDI-TOF mass spectra recorded for chimeric PS-oligonucleotides. CCDC 2063388. For ESI and crystallographic data in CIF or other electronic format see https://doi.org/10.1039/d2ra04855h

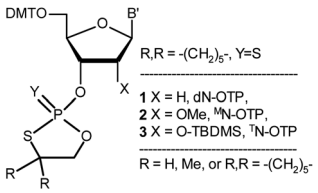

Chart 1 Classes of the OTP derivatives of 2′-deoxyribo- and ribonucleosides. B′ = Ade^{Bz}, Cyt^{Bz}, Gua^{iBu}, or Ura. For those with R = H or Me, see ref. 13 and 16, respectively.

oligonucleotide decamer synthesized by a non-stereocontrolled method exists as a mixture of $2^9 = 512$ P-diastereomers, and the content of a single diastereomer is less than 0.2%. Since each P-diastereomer can interact with a biological target (usually with fixed chirality) in slightly different ways, the mixtures of hundreds of P-diastereomers may be useless for detecting the interactions of interest. To overcome this problem, stereocontrolled synthetic methods have been developed.[13–15] Among them, the approach utilizing so called oxathiaphospholane monomers (OTP; developed in this laboratory)[13,16] has yielded the most P-stereodefined oligomers so far, and some of them showed interesting P-stereodependent properties in biochemical studies.[17–21] So far, the OTP method has mainly used separated P-diastereomers of 3′-*O*-(2-thio-4,4-pentamethylene-1,3,2-oxathiaphospholane) derivatives of 2′-deoxyribonucleosides (**1**, X = H, Y = S, R,R = –(CH$_2$)$_5$–, Chart 1), although 2-selena monomers (**1**, X = H, Y = Se, R,R = –(CH$_2$)$_5$–) have been used in the synthesis of P-stereodefined phosphoroselenoate analogs of DNA.[22] In 1996, a set of four monomers **3** (X = *O*-TBDMS, R = H) was synthesized and chromatographically separated into P-diastereomers.[23] They were used in the solid-phase synthesis of dinucleoside phosphorothioates N$_{PS}$N, which were obtained in 66–98% yields. However, the separation of *fast*- and *slow*-eluting monomers was very difficult and inefficient. In other attempts to synthesize P-stereodefined [PS]-RNA, the synthesis of up to 10-mers was achieved using a method based on nucleoside-3′-*O*-oxazaphospholidine monomers with the 2′-*O*-TBDMS protecting group.[24] Good coupling yields (97–99%) were observed, but stereoselectivity was not perfect (≥96 : 4). A diastereoselectivity ≥98 : 2 was observed when oxazaphospholidine monomers with 2′-*O*-(2-cyanoethoxymethyl) group were used.[25]

This discovery prompted our attempt to develop a fully stereospecific method for the synthesis of [PS]-(2′-OMe)-RNA ([PS]-^{M}RNA) and [PS]-RNA oligonucleotides with P-stereodefined phosphorothioate internucleotide linkages. (For simplicity the (2′-OMe)-, (2′-*O*-TBDMS)-, 2′–OH– and 2′-deoxyribonucleosides will be referred to as ^{M}N, ^{T}N, N, and dN, respectively). In a next step we will attempt to develop a method for the synthesis of {[PO]-DNA:[PS]-^{M}RNA},‡ {[PO]-DNA:[PS]-RNA}, and {[PO]-RNA:[PS]-RNA} chimeras that could be used as model compounds in biochemical studies.

‡ A colon in structures such as {[PO]-RNA:[PS]-RNA} or [PS]-{DNA:^{M}RNA} indicates that the nucleotides of both types are contained in the same oligonucleotide strand.

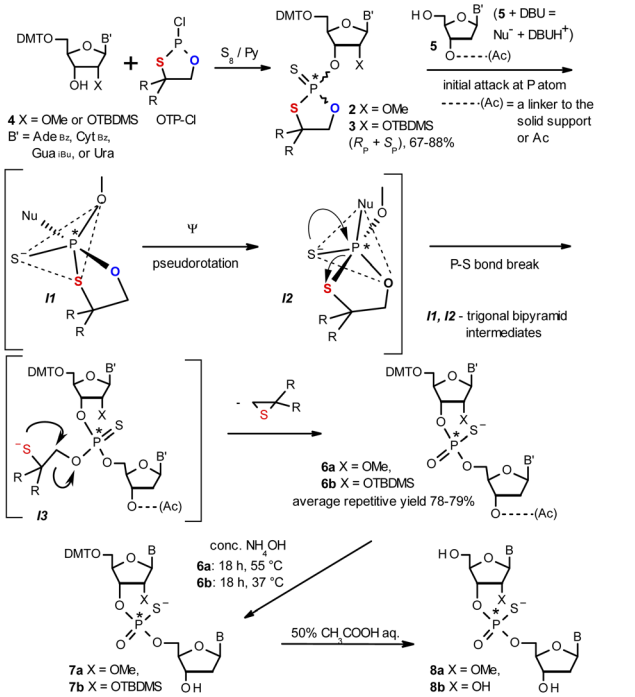

Scheme 1 Synthesis of OTP monomers **2** and **3** (R,R = –(CH$_2$)$_5$–) and the mechanistic principle of the coupling step.

In this report, we present the synthesis of OTP monomers **2** (X = OMe, ^{M}N-OTP, Chart 1) and **3** (X = *O*-TBDMS, ^{T}N-OTP) and their separation into pure P-diastereomers, as well as the result of the successful crystallographic analysis of detritylated **3a** (B′ = Ade^{Bz}). The P-diastereomerically pure monomers **2** and **3** were used for the synthesis of chimeric dinucleotides **8a** and **8b**, respectively (Scheme 1), and the absolute configuration of the P atoms was determined enzymatically. Melting curves were recorded to determine the thermal stability of duplexes formed by P-stereodefined chimeric [PS]-{DNA:^{M}RNA} and [PS]-{DNA:RNA} oligonucleotides (10 nt in length) with Watson–Crick paired DNA and ^{M}RNA matrices.

Results and discussion

The mechanistic principle of the OTP method

The synthesis of OTP monomers **2** and **3** and the mechanistic principle of the coupling step are shown in Scheme 1. It has been documented[26] that the condensation does not follow a stereoinvertive S$_N$2P mechanism but is a stereoretentive process. The initial attack of a nucleoside **5** occurs from the side opposite to the most electronegative atom bonded to the phosphorus center (the oxygen atom in the oxathiaphospholane ring of **2** or **3**, marked in blue; Scheme 1) to form a trigonal bipyramidal intermediate ***I1***. Subsequently, a pseudorotation process furnishes the intermediate ***I2***, in which the thioalkyl leaving group occupies the axial position, followed by cleavage of the P–S bond to form the triester intermediate ***I3***. The condensation process concludes with the elimination of episulfide. Finally, deprotection of the resulting intermediates **6** and

7 and purification steps yield [PS]-oligomers **8**. The range of P-stereodefined phosphorothioate oligonucleotides was extended by the synthesis of [PS]-LNA[27] and [PS]-GNA[28] oligomers as well as oligomers containing 3′-amino-2′,3′-dideoxy nucleosides ([NPS]-DNA).[29] Unfortunately, oligomers of the latter two series were obtained in low yields due to unexpected side reactions and unfavorable conformational factors.

Preparation of P-diastereomerically pure ^{M}N-OTP and ^{T}N-OTP monomers

Protected ribonucleosides **4** (Scheme 1, B′ = Ade^{Bz}, Cyt^{Bz}, Gua^{iBu}, or Ura; X = OMe or *O*-TBDMS), were phosphitylated with 2-chloro-4,4-pentamethylene-1,3,2-oxathiaphospholane (OTP-Cl, 1.2 equiv.) and then sulfurized with elemental sulfur.[30] The resultant monomers **2** and **3** were isolated in 67–88% yields. The P-diastereomers (formed in nearly equimolar amounts) were separated by preparative HPLC on a silica gel column (Fig. S1a and b, ESI†), and their structures were confirmed by HR MS (Fig. S2a–h and S3a–h, ESI†). (For ^{1}H, ^{13}C and ^{31}P NMR spectra see ESI, Fig. S4–S6,† respectively). Interestingly, ^{31}P NMR analysis (Tables 1 and 2) showed that all *fast*-eluting isomers of **3** had lower chemical shifts (δ) than their *slow*-eluting counterparts (as observed for dN-OTP monomers[16] and LNA-OTP[27]) whereas this relationship was reverse for compounds **2**.

X-ray crystallography analysis of the detritylated oxathiaphospholane monomer 3a (B′ = Ade^{Bz})

Previously published results on the hydrolysis of dinucleotides d(N$_{PS}$N) with snake venom phosphodiesterase (svPDE) and nuclease P1 (nP1) (R_P- and S_P-specific phosphodiesterase, respectively) showed that the compounds obtained from *fast*- and *slow*-eluting monomers dN-OTP (**1**, X = H, Y = S, R = Me or R,R = –(CH$_2$)$_5$–) contain the internucleotide bonds with the P atoms of the absolute configuration R_P and S_P, respectively.[16] The same correlation was found for the analogous OTP derivatives of LNA nucleosides.[27] X-ray analysis of LNA-thymidine-3′-*O*-(2-thio-4,4-pentamethylene-1,3,2-oxathiaphospholane) confirmed the stereoretentive course of the condensation step. The "locked" structure naturally resulted in the C3′-*endo* conformation of the sugar ring.

In the present studies, a crystal suitable for X-ray analysis was obtained from the 5′-OH deprotected *fast*-eluting monomer **3a** (B′ = Ade^{Bz}). Detritylation was carried out in anhydrous acetonitrile using a sodium hydrogen sulfate suspension deposited on silica gel.[31] The crystal structure was resolved (Fig. 1) with the refinement parameter $R = 0.0563$ and ESI.† The

Table 1 Characteristics of the ^{M}N-OTP monomers **2a–d**

	^{M}A-OTP (**2a**)	^{M}C-OTP (**2b**)	^{M}G-OTP (**2c**)	^{M}U-OTP (**2d**)
Yield[a] (%)	78	88	69	83
Rf[b] (TLC)	0.72	0.83	0.70	0.81
Eluent for TLC/HPLC[c]	80 : 20	70 : 30	100	40 : 60
MM calc. (Da)	893	869	875	766
For *fast*-2/*slow*-2				
Rt[d] (min)	16/24	13/18	12/17	19/26
HR MS[e] (*m*/*z*)	892.2630/892.2625	868.2510/868.2510	874.2706/874.2715	765.2079/765.2082
δ ^{31}P NMR[f] (ppm)	106.555/106.132	106.690/106.579	107.042/106.688	106.719/106.571

[a] Yield of the isolated mixture of P-diastereomers. [b] Eluent $CHCl_3$: MeOH (9 : 1, v/v). [c] Separation of P-diastereomers at an AcOEt : hexane ratio (v/v). [d] A Phenomenex Luna 5u Silica gel column (100 Å; 250 × 10 mm; flow rate 5 mL min^{-1}, isocratically). [e] Recorded with a SYNAPT G2-Si High Definition Mass Spectrometer. [f] In anhydrous $CDCl_3$.

Table 2 Yield, chromatographic and spectroscopic data for the ^{T}N-OTP monomers **3a–d**

	^{T}A-OTP (**3a**)	^{T}C-OTP (**3b**)	^{T}G-OTP (**3c**)	^{T}U-OTP (**3d**)
Yield[a] (%)	70	72	67	73
Rf[b] (TLC)	0.64	0.74	0.62	0.71
Eluent for TLC/HPLC[c]	50 : 50	70 : 30	100	40 : 60
MM calc. (Da)	993	969	975	866
For *fast*-3/*slow*-3				
Rt[d] (min)	15/17	35/40	10/15	25/35
HR MS[e] (*m*/*z*)	992.3309/992.3311	968.3198/968.3192	974.3427/974.3418	865.2776/865.2775
δ ^{31}P NMR[f] (ppm)	105.880/107.519	106.966/107.022	106.244/107.342	106.500/107.369

[a] Yield of the isolated mixture of P-diastereomers. [b] Eluent $CHCl_3$: MeOH (9 : 1, v/v). [c] Separation of P-diastereomers at an AcOEt : hexane ratio (v/v). [d] A Phenomenex Luna 5u Silica gel column (100 Å; 250 × 10 mm; flow rate 5 mL min^{-1}, isocratically). [e] Recorded with a SYNAPT G2-Si High Definition Mass Spectrometer. [f] In anhydrous $CDCl_3$.

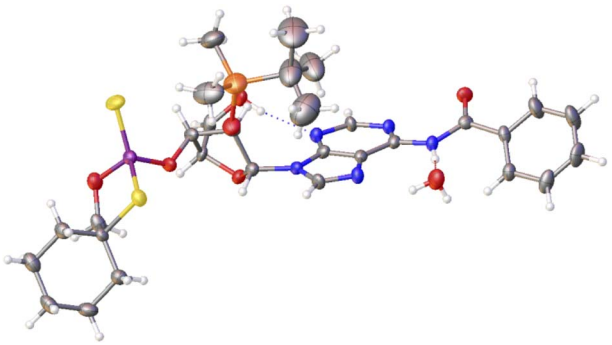

Fig. 1 X-ray ORTEP diagram of the detritylated *fast*-eluting P-diastereomer of **3a** showing the R_P absolute configuration. The displacement ellipsoids are shown at the 50% probability level.[32] Colors: red – oxygen, blue – nitrogen, pink – phosphorus, yellow – sulfur, orange – silicon, black – carbon, white – hydrogen.

crystal data and the data acquisition and refinement parameters are listed in Table S1 (ESI†). It should be noted that despite the presence of a 2′-oxygen atom, the (normally strong) anomeric effect is not decisive in this case and the sugar ring exists in the C2′-*endo* conformation (Fig. 2), perhaps due to the steric requirements of the bulky TBDMS group.

Crystallization experiments with all other DMT-labeled as well as detritylated OTP derivatives were unsuccessful.

Synthesis and enzymatic analysis of $^{M}N_{PS}T$ and $N_{PS}T$ dinucleotides

Since X-ray analysis was successful only for the derivative of *fast*-eluting **3a**, enzymatic analysis was performed to complete the stereochemical assignment in the remaining **2** and **3**. For this purpose, 4 pairs of P-diastereomeric diesters $^{M}N_{PS}T$ (**6a**, X = OMe) and 4 pairs of P-diastereomeric diesters $N_{PS}T$ (**6b**, X = OH) were prepared from 3′-*O*-acetyl-thymidine (**5**, B′ = Thy, Scheme 1) and diastereomerically pure (*fast*- or *slow*-eluting) ^{M}N-OTP **2a–d** or ^{T}N-OTP **3a–d**, respectively. The base-labile protecting groups in intermediates **6** were removed with concentrated ammonia. Subsequently, products **7a** (X = OMe; derived from **2**) were routinely detritylated with 50% $AcOH_{aq}$. The DMT and TBDMS moieties in the freeze-dried products **7b** (X = *O*-TBDMS; derived from **3**) were removed by treatment with 3HF × NEt_3. The MALDI TOF MS data for the resulting dinucleotides **8a** and **8b** are given in Table 3.

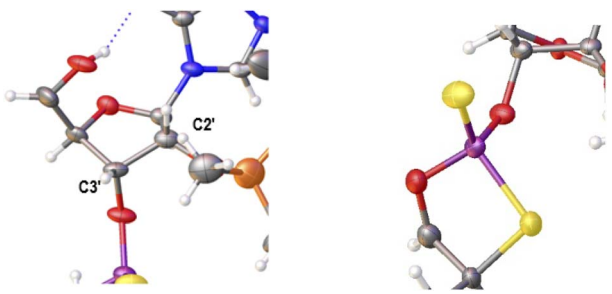

Fig. 2 Parts of the X-ray ORTEP diagram show: left image–a DNA-like C2′-*endo* conformation of detritylated *fast*-eluting **3a**; right image – spatial orientation of substituents on the phosphorus atom. Colors as in Fig. 1.

Table 3 MALDI TOF MS data for $^{M}N_{PS}T$ **8a** (X = OMe) and $N_{PS}T$ (**8b**, X = OH) synthesized from P-diastereomerically pure ^{M}N-OTP **2a–d** and ^{T}N-OTP **3a–d**, respectively

^{M}N-OTP (**2a–d**) or ^{T}N-OTP (**3a–d**)		MALDI TOF MS *m/z* [m/z_{calc}]	
B′	Isomer	$^{M}N_{PS}T$ (**8a**, X = OMe)	$N_{PS}T$ (**8b**, X = OH)
Ade^{Bz}	*Fast*	600.1283 [601]	586.1066 [587]
	Slow	600.1283 [601]	586.1064 [587]
Cyt^{Bz}	*Fast*	576.1171 [577]	562.1013 [563]
	Slow	576.1174 [577]	562.1011 [563]
Gua^{iBu}	*Fast*	616.1229 [616]	602.1076 [602]
	Slow	616.1232 [616]	602.1074 [602]
Ura	*Fast*	577.1006 [578]	563.0858 [564]
	Slow	577.1007 [578]	563.0848 [564]

Small amounts (2–3 OD_{254} units) of all 16 P-diastereomeric dinucleotides **8** were isolated using RP-HPLC and further treated with the svPDE and nP1 enzymes, which are R_P- and S_P-stereoselective, respectively. Subsequent RP-HPLC analysis revealed that all dinucleotides **8** obtained from the *fast*-eluting **2a–d** and **3a–d** were hydrolyzed with svPDE and not with nP1. Their counterparts obtained from the *slow*-eluting monomers were hydrolyzed with nP1 and not with svPDE. These results, together with the X-ray data collected for **3a**, confirm the stereoretentive course of the condensation step.

Relative reactivity of ^{M}N-OTP and ^{T}N-OTP compared with dN-OTP

It has been reported previously that when monomers **1** were used, 92–94% yields were observed with single coupling, allowing 18–23 nt long PS-DNA oligomers to be assembled.[18] Previous experiments with the OTP derivatives of LNA nucleosides showed that double coupling was necessary to achieve an acceptable yield of the condensation step.[27] Using this modified protocol, chimeric [PS]-{DNA:LNA} oligomers were obtained with LNA units in every third position.§ This lower reactivity was tentatively attributed to steric hindrance due to the C2′–O–CH_2–C4′ bridge near the reacting phosphorus center. However, unsatisfactory attempts to synthesize oligomers with 3′-amino-2′,3′-dideoxy nucleosides ([NPS]-DNA)[29] and subsequent molecular modeling experiments indicated the importance of the deoxyribose ring conformation in the OTP monomers. Importantly, only the OTP derivative of 3′-amino-3′-deoxythymidine allowed the synthesis of [NPS]-DNA 8-mer, while none of the monomers with the other three nucleobases allowed more than four coupling steps. Therefore, competition experiments were performed to determine the relative reactivity of selected purine and pyrimidine monomers **2** and **3** compared

§ Uniformly modified [PS]-LNA oligomers were not synthesized because of expected too strong rigidity of the resultant strand.

Table 4 The composition (mol%, by ^{31}P NMR) of the mixtures of ^{M}N-OTP/dN-OTP and ^{T}N-OTP/dN-OTP used in the reaction with thymidine attached to the solid support, and the composition (mol%, by HPLC) of the resultant mixtures of dinucleotides $^{M}N_{PS}T$/$dN_{PS}T$ and $^{T}N_{PS}T$/$dN_{PS}T$

	N = A		N = U	
OTP substrates, dinucleotide products[ab]	*Fast*	*Slow*	*Fast*	*Slow*
^{M}N-OTP (**2**) : dN-OTP (**1**)	49 : 51	44 : 56	53 : 47	46 : 54
$^{M}N_{PS}T$: $dN_{PS}T$	26 : 74	42 : 58	31 : 69	32 : 68
Selectivity ratio[c]	0.36	0.91	0.40	0.55
^{T}N-OTP (**3**) : dN-OTP (**1**)	42 : 58	44 : 56	53 : 47	55 : 45
$^{T}N_{PS}T$[d] : $dN_{PS}T$	22 : 78	6 : 94	19 : 81	15 : 85
Selectivity ratio[c]	0.39	0.08	0.21	0.14

[a] The dinucleotide products were detritylated before cleavage from the solid support. [b] In the adenosine containing products, the benzoyl protecting group was removed with concentrated ammonia. [c] The selectivity ratios are calculated by dividing % composition of products by % composition of substrates. [d] The TBDMS group in $^{T}N_{PS}T$ dinucleotides was not removed.

to the corresponding dN-OTP. For this purpose, the approximately equimolar mixtures **1**/**2** and **1**/**3** (measured by ^{31}P NMR) were reacted with thymidine bound to a solid support (10 mg of each OTP monomer was used, *i.e.*, a 14–18-fold excess). The resultant $^{M}N_{PS}T$/$dN_{PS}T$ and $^{T}N_{PS}T$/$dN_{PS}T$ mixtures were detritylated, detached from the solid support, deprotected with concentrated ammonia (the TBDMS group in the $^{T}N_{PS}T$ dinucleotides was not removed), and analyzed using RP-HPLC. The required standards were prepared independently. The results (Table 4) generally show that the ^{M}N-OTP monomers studied were two to three times less reactive compared with the corresponding dN-OTP, as the selectivity ratio values (calculated by dividing the percent composition of the dinucleotide products by the percent composition of the OTP substrates) ranged from 0.36 to 0.55. Only for the *slow*-eluting ^{M}A-OTP the difference was almost negligible (Table 4, selectivity ratio 0.91, double underlined). The reactivity of ^{T}N-OTP was 5–12 times lower, with the lowest selectivity ratio value of 0.08 (Table 4, underlined). Reactivity comparable to ^{M}N-OTP was found only for the *fast*-eluting ^{T}A-OTP (selectivity ratio 0.39).

The generally low reactivity observed for **2** and **3** suggested that the synthesis protocol optimized for [PS]-DNA[34] and later modified for the synthesis of [PS]-LNA oligomers[27] would be inadequate. In addition, the widely varying selectivity ratios indicated that several factors might influence reactivity, so that optimization of the protocol for all 16 diastereomers of ^{M}N-OTP and ^{T}N-OTP would be a lengthy process with uncertain prospects for success. An attempt to synthesize uniformly modified [PS]-(^{M}A)$_4$T, in which the most reactive *slow*-eluting ^{M}A-OTP (**2a**, see Table 4) was double-coupled (thymidine was bound to the support), yielded only a small amount of product. The results of the DMT cation assay, shown in Fig. 3 (green line), clearly indicate that although the first coupling was carried out with 86% yield, the next three coupling steps were much less efficient with 74, 67 and 49% yield, respectively. The synthesis of [PS]-(^{M}A)$_4$T showed that the synthesis of [PS]-^{M}RNA and [PS]-RNA oligomers with mixed sequences and longer than penta- or hexamers will be very difficult.

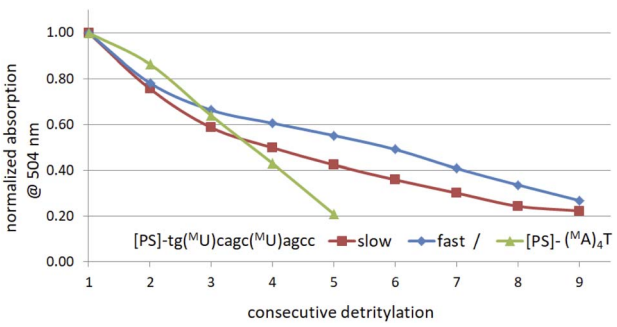

Fig. 3 Decay of absorption (at 504 nm) of the DMT-cation released in consecutive detritylation steps.

Synthesis and properties of chimeric [PS]-{DNA:^{M}RNA} and [PS]-{DNA:RNA} oligonucleotides

Because of the relatively low repetitive yield of coupling steps in syntheses with monomers **2** or **3**, we focused on the synthesis of P-stereodefined chimeric [PS]-{DNA:^{M}RNA} and [PS]-{DNA:RNA} oligonucleotide decamers (collectively referred to as [PS]-chimeras or PSCh) with base sequence 5′-tgtcagctag-3′, where lowercase letters represent DNA units. In the sequences of analogous chimeric oligomers, the introduced N_{PS} are indicated in uppercase letters (*e.g.* A or U), whereas the $^{M}N_{PS}$ units are indicated in uppercase letters with a superscript M prefix (*e.g.* ^{M}A or ^{M}U).

In the synthesis of each oligomer, the dN-OTP monomer was replaced in two selected cycles by ^{M}N-OTP or ^{T}N-OTP carrying the same nucleobase, except for the T-OTP monomer, which was replaced by ^{M}U-OTP or ^{T}U-OTP congeners. The codes, specific sequences, and HR MS data for two synthesized reference [PS]-DNA and sixteen chimeric [PS]-oligomers are listed in Table 5. [Note: in codes such as **UR** or **^{M}US**, the capital letters **R** or **S** denote [PS]-oligomers with phosphorus atoms with either R_P or S_P absolute configuration, respectively].

The DMT cation decay assay was performed for each synthesis, and calculations for the steps using ^{M}N-OTP or ^{T}N-OTP (double coupling was performed) gave the average coupling yields of 78 and 79%, respectively (Table S2, ESI†). After cleavage from the support and removal of the base-labile protecting groups, the DMT-labeled oligomers were purified

Table 5 Codes, sequences, and HR MS characteristics of the [PS]-DNA and chimeric [PS]-{DNA:^{M}RNA} and [PS]-{DNA:RNA} oligomers under study

Code	[PS]-oligomer[a] sequence (5′ → 3′)	MS ES (*m*/*z*) Calc.	Found
[PS]-DNA from 1a–d			
BR	tgtcagctag	3185.34	3185.3401
BS	tgtcagctag	3185.34	3185.3301
[PS]-{DNA:^{M}RNA} from 1a–d and 2a–d			
^{M}AR	tgtc^{M}Agct^{M}Ag	3245.36	3245.3501
^{M}AS			3245.3501
^{M}CR	tgt^{M}Cag^{M}Ctag	3245.36	3245.3401
^{M}CS			3245.3500
^{M}GR	t^{M}Gtca^{M}Gctag	3245.36	3245.4001
^{M}GS			3245.3401
^{M}UR	tg^{M}Ucagc^{M}Uag	3217.33	3217.3000
^{M}US			3217.3000
[PS]-{DNA:RNA} from 1a–d and 3a–d			
AR	tgtcAgctAg	3217.33	3217.3181
AS			3217.3101
CR	tgtCagCtag	3217.33	3217.3101
CS			3217.3000
GR	tGtcaGctag	3217.33	3217.3101
GS			3217.3101
UR	tgUcagcUag	3189.30	3189.3000
US			3189.3000

[a] In the sequences, the units containing 2′-deoxyribo- and ribonucleosides are indicated in lowercase and uppercase letters, respectively. The $^{M}N_{PS}$ units are marked with a superscript M prefix (^{M}N).

by RP-HPLC, and the collected samples were detritylated and isolated by RP-HPLC. Fig. 4 shows typical chromatograms recorded during the DMT-ON and DMT-OFF purification steps; here those for **^{M}GS** (S_P). MALDI TOF MS spectra for PSCh are shown in ESI.†

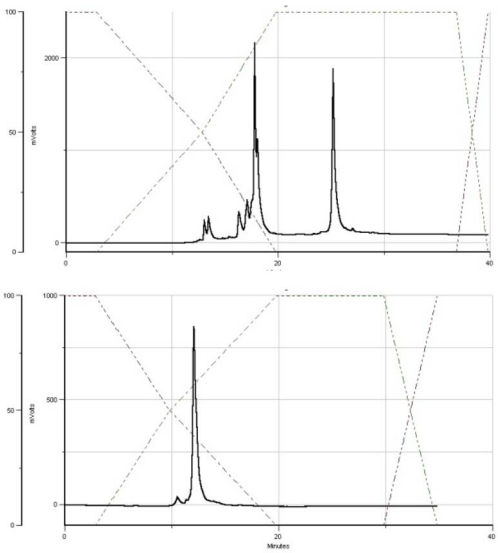

Fig. 4 HPLC profiles recorded for **^{M}GS** during DMT-ON (the upper panel) and DMT-OFF (the lower panel) purification steps.

Melting experiments for canonical and hybrid duplexes

For the melting experiments, the oligomers were mixed with the equimolar amount of Watson–Crick-paired DNA matrix (**Md**) or mRNA matrix (**Mm**) (2.0 μM concentration each) in pH 7.2 buffer. The observed changes in UV absorbance followed the two-state mechanism and the recorded curves had the expected S-shape. An example set of melting curves is shown in Fig. 5. Melting temperatures (compiled in Table 6) were calculated using the numerical fitting method provided by the UV spectrophotometer manufacturer. The ΔT_m values were calculated by subtracting the control T_m from the values recorded for the duplexes tested.

Melting experiments for duplexes formed by [PO]-chimeras

When analyzing the results of melting experiments with duplexes formed by [PO]-{DNA:^{M}RNA} chimeras (**^{M}A**, **^{M}C**, **^{M}G**, and **^{M}U**), an oligonucleotide with the sequence [PO]-5′-tgtcagctag-3′ (**B**asal **D**NA oligomer, **Bd**) was used as a reference. Compared to the reference **Bd**/**Md** duplex (T_m = 41 °C, Table 6), the [PO]-{DNA:^{M}RNA}/**Md** duplexes were 1 ÷ 9 °C less thermally stable (T_m = 32 ÷ 40 °C, Fig. 6, green bars), with the pyrimidine units ($^{M}C_{PO}$, $^{M}U_{PO}$) destabilizing the duplexes more than the purine units.

Melting experiments with the **Mm** matrix showed that the purine units ($^{M}A_{PO}$, $^{M}G_{PO}$) slightly stabilized the duplexes (ΔT_m = 1 ÷ 4 °C, Fig. 6, black bars), compared to the reference **Bd**/**Mm** duplex (T_m = 51 °C). The duplexes containing the $^{M}C_{PO}$ or $^{M}U_{PO}$ nucleotides were less stable than **Bd**/**Mm** and the destabilizing effect was strongest for **^{M}U** (ΔT_m = −5 °C). These results differ from those of Wengel and coworkers, who showed that one to three LNA nucleotides introduced into the DNA strand at either the adenine (5′-AGCACCAG) or thymine (5′-TGCTCCTG) residues increased the thermal stability of the corresponding {DNA:LNA}/RNA heteroduplexes in 110 mM Na^+ buffer.[33] For two introduced A-LNA or T-LNA units, ΔT_m = 10 and 16 °C, respectively, were found. It can be argued that RNA matrices were used in these experiments, but Dolot and coworkers showed that crystals of DNA/RNA and DNA/^{M}RNA duplexes have very similar geometries.[34]

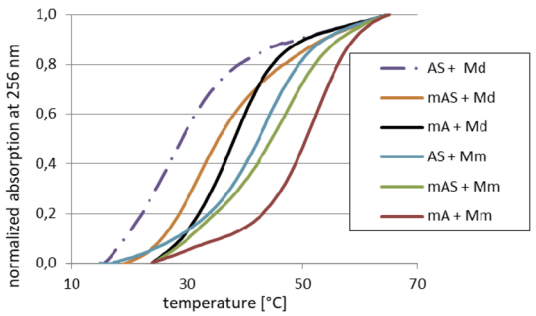

Fig. 5 Normalized melting curves for selected duplexes (see legend) dissolved in pH 7.2 buffer (10 mM Tris–HCl, 100 mM NaCl, and 10 mM $MgCl_2$). The curves designations **mA** and **mAS** (in the legend) correspond to **^{M}A** and **^{M}AS**, respectively.

Table 6 Melting temperatures derived from the melting profiles recorded at pH 7.2 for [PO]- or [PS]-oligomers mixed with the Watson–Crick paired DNA (**Md**) or (2′-OMe)-RNA (**Mm**) matrices at a 1 : 1 molar ratio

		Md		**Mm**	
Code	Sequence (5′ → 3′)[a]	T_m [°C]	ΔT_m [°C]	T_m [°C]	ΔT_m [°C]
[PO]-DNA reference oligomer					
Bd	tgtcagctag	41	—	51	—
[PO]-{DNA:^{M}RNA} chimeras[b]					
^{M}A	tgtc^{M}Agct^{M}Ag	38	−3	52	+1
^{M}C	tgt^{M}Cag^{M}Ctag	36	−5	48	−3
^{M}G	t^{M}Gtca^{M}Gctag	40	−1	55	+4
^{M}U	tg^{M}Ucagc^{M}Uag	32	−9	46	−5
[PS]-DNA reference oligomers					
BR	tgtcagctag	35	—	32	—
BS		35	—	35	—
[PS]-{DNA:RNA} chimeras[c]					
AR	tgtcAgctAg	30	−5	40	+8
AS		27	−8	43	+8
CR	tgtCagCtag	30	−5	38	+6
CS		34	−1	39	+4
GR	tGtcaGctag	31	−4	39	+7
GS		30	−5	37	+2
UR	tgUcagcUag	27	−8	40	+8
US		31	−4	40	+5
[PS]-{DNA:^{M}RNA} chimeras[c]					
^{M}AR	tgtc^{M}Agct^{M}Ag	30	−5	44	+12
^{M}AS		32	−2	47	+12
^{M}CR	tgt^{M}Cag^{M}Ctag	31	−4	41	+9
^{M}CS		32	−4	39	+4
^{M}GR	t^{M}Gtca^{M}Gctag	30	−5	46	+14
^{M}GS		31	−4	48	+13
^{M}UR	tg^{M}Ucagc^{M}Uag	29	−6	40	+8
^{M}US		24	−11	41	+6

[a] In the sequences, the DNA and RNA units are written in lowercase and uppercase letters, respectively. The ^{M}N$_{PS}$ units are marked with a superscript M prefix (^{M}N). [b] The ΔT_m values were calculated using the T_m values for the corresponding duplexes **Bd**/**Md** or **Bd**/**Mm**. [c] The ΔT_m values were calculated using the T_m values for the corresponding duplexes **B(R,S)**/**Md** or **B(R,S)**/**Mm**.

Melting experiments for the PSCh/Md duplexes. The basal complexes **BR**/**Md** and **BS**/**Md** (P-stereodefined [PS]-DNA/DNA; collectively referred to as **B(R,S)**/**Md**) were equally stable (T_m = 35 °C). Compared with the phosphate **B**/**Md** reference complex, they were 6 °C less thermally stable (Table 6). Compared with **B(R,S)**/**Md**, in all cases, regardless of the absolute configuration of the P atoms, ribonucleotide units (N$_{PS}$) as well as (2′-OMe)-ribonucleotide units (^{M}N$_{PS}$) present in the P-stereodefined [PS]-chimeras further reduced the thermal stability of the duplexes (Fig. 6, blue bars), as the ΔT_m values ranged from −1 °C for the most stable duplex CS/**Md** (T_m = 34 °C) to −11 °C for ^{M}US/Md (T_m = 24 °C). Within groups of [PS]-oligonucleotides carrying ^{M}N$_{PS}$ or N$_{PS}$ with the same nucleobase (*e.g.*, ^{M}AR, ^{M}AS, AR, and AS) the patterns of changes were different.

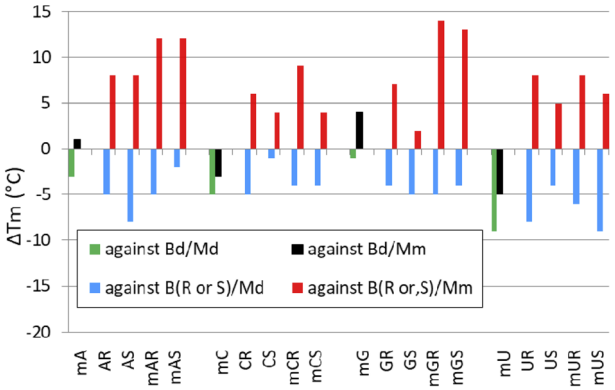

Fig. 6 Changes in melting temperature of duplexes (ΔT_m; °C) formed by [PO]-{DNA:^{M}RNA} chimeras with **Md** (green bars) or **Mm** (black bars), and PSCh oligomers with **Md** (blue bars) and **Mm** (red bars). The ΔT_m values were calculated using the T_m values for the corresponding duplexes **Bd**/**Md**, **Bd**/**Mm**, **B(R,S)**/**Md** and **B(R,S)**/**Mm**. Designations along the horizontal axis such as **mAR** or **mGS** correspond to ^{M}**AR** and ^{M}**GS**, respectively.

Melting experiments for the PSCh/Mm duplexes. The **BR**/**Mm** and **BS**/**Mm** complexes (collectively referred to as **B(R,S)**/**Mm**) had T_m = 32 and 35 °C, respectively (Table 6), and were similarly stable to **B(R,S)**/**Md**. Compared with the phosphate **B**/**Mm** reference complex, they were less stable by 19 and 16 °C, respectively. In contrast to the PSCh/**Md** duplexes, the use of the (2′-OMe)-RNA matrix (**Mm**) resulted in an increase in the thermal stability of the duplexes. The most stable ^{M}**GS**/**Mm** had T_m = 48 °C, but compared to **B(R,S)**/**Mm** the largest ΔT_m = 14 °C was observed for ^{M}**GR**/**Mm** (Fig. 6, red bars), while the smallest effect (ΔT_m = 2 °C) was observed for **GS**/**Mm**. The complexes formed by **Mm** with PSCh containing ^{M}N$_{PS}$ units (especially those containing the purine derivatives) were more stable than those with PSCh containing the N$_{PS}$ nucleotides. Within groups of [PS]-oligonucleotides carrying ^{M}N$_{PS}$ or N$_{PS}$ with the same nucleobase the patterns of changes were different.

Summary of melting experiments. The analysis of the ΔT_m values obtained from the melting experiments (they are shown in Fig. 6) leads to three conclusions. First, compared to **B(R,S)**/**Md** and **B(R,S)**/**Mm**, the ^{M}N$_{PS}$ and N$_{PS}$ units present in PSCh decreased the thermal stability of duplexes formed with **Md** and increased the stability of those formed with **Mm**. Second, the strongest stabilizing effects (ΔT_m > 10 °C) were caused by purine ^{M}N$_{PS}$ residues in oligonucleotides interacting with **Mm**. Third, the changes in thermal stability of duplexes formed by PSCh with **Md** and **Mm** did not correlate with the absolute configuration of phosphorus atoms. For example, ΔT_m for **GR**/**Mm** is 5 °C larger than for **GS**/**Mm**, whereas the ΔT_m values for **AR**/**Mm** and **AS**/**Mm** and for ^{M}**AR**/**Mm** and ^{M}**AS**/**Mm** are the same (8 and 12 °C, respectively). However, the ΔT_m for the duplexes formed by PSCh with the S_P absolute configuration of phosphorus atoms were in no case larger than for the duplexes with their R_P counterparts.

Conclusions

The 2-thio-1,3,2-oxathiaphospholane monomers of 2′-OMe and 2′-*O*-TBDMS series (^{M}N-OTP and ^{T}N-OTP, **2** and **3**, respectively)

were synthesized in good yield and effectively separated into pure P-diastereomers. The X-ray crystallographic analysis revealed the R_P absolute configuration of the phosphorus atom in the *fast*-eluting diastereomer **3a** (B′ = Ade^{Bz}). Using the R_P-selective phosphodiesterase svPDE and the S_P-selective Nuclease P1 it was found that in both monomer series the *fast*- and *slow*-eluting P-diastereomers are precursors of dinucleotides with R_P and S_P absolute configuration of the phosphorus atoms, respectively. Importantly, no traces of P-epimerization were observed during coupling steps. P-Stereodefined chimeric [PS]-{DNA:^{M}RNA} and isosequential [PS]-{DNA:RNA} 10-mer oligomers with two $^{M}N_{PS}$ or N_{PS} units were synthesized. Melting experiments using complexes with Watson–Crick paired DNA matrix showed that $^{M}N_{PS}$ or N_{PS} units decrease the thermal stability of the duplexes ($\Delta T_m = -0.5 \div -5.5$ °C per modification), regardless of the absolute configuration of the P-atoms. When the (2′-OMe)-RNA matrix was used an increase in T_m was observed in all cases ($\Delta T_m = +1 \div +7$ °C per modification). The changes in thermal stability of duplexes formed by [PS]-chimeras with DNA and (2′-OMe)-RNA matrices did not correlate with the absolute configuration of phosphorus atoms.

Despite of double-coupling, the average repetitive yields of the condensation steps with either **2** or **3** were rather moderate (78–79%). Nevertheless, even these moderate yields should allow the synthesis of {[PO]-DNA:[PS]-^{M}RNA} and {[PO]-RNA:[PS]-RNA} chimeras that could be used as model compounds in biochemical studies. To achieve this goal, the conditions for an effective combination of phosphoramidite and OTP synthesis methods need to be worked out. This work is in progress.

Experimental section

^{1}H NMR and ^{31}P NMR spectra were acquired using Bruker instruments (AV-200, DRX-500, or Avance Neo 400; operating for ^{1}H at 200, 500, and 400 MHz, respectively). Chemical shift (δ) values are in ppm, referenced to internal tetramethylsilane (TMS) or residual solvent protons for ^{1}H NMR and external 85% H_3PO_4 for ^{31}P NMR.

High-resolution mass spectra (HR MS) were acquired using a Synapt G2 Si mass spectrometer (Waters Corporation, Milford, MA) equipped with an ESI source and a quadrupole time-of-flight mass analyzer. Measurements were performed in negative ion mode with the capillary and sampling cone voltages set at 2.7 kV and 20 V, respectively. The temperature of the source was 110 °C. To ensure satisfactory accuracy, data were acquired in a centroid mode and readings were corrected during acquisition using leucine-enkephalin as an external reference (LockSprayTM) generating reference ions at *m*/*z* 554.2615 Da ([M–H]$^-$) in negative ESI mode. Data sets were processed using MassLynx 4.1 software (Waters).

MALDI-TOF MS analyses of oligonucleotides were performed with negative ion detection using a Voyager Elite instrument (PerSeptive Biosystems Inc, Framingham, MA) operating in reflector mode or an Axima Performance instrument (Shimadzu Biotech Corp., Japan) operating in linear mode.

TLC silica gel 60 plates F254 developed in $CHCl_3$/MeOH, 9 : 1 (v/v), were used for routine analyses. HP TLC Silica gel 60 plates with a UV-F_{254} indicator were used to evaluate the separability of the P-diastereomers of **2** and **3**.

A Varian binary HPLC system (two PrepStar 210 pumps, 25 mL pump heads, one ProStar 320 UV/vis detector at 275 nm) was used for HPLC separation of the P-diastereomers of monomers **2** and **3**. A Phenomenex Luna 5 μm silica column (100 Å; 250 × 10 mm; flow rate 5 mL min^{-1}) was used in search of the appropriate conditions. Preparative separation was performed with a Pursuit XRs silica gel column (10 μm, 250 × 21.2 mm) eluted at a flow rate of 25 mL min^{-1}. Gradient-grade HPLC solvents from Sigma-Aldrich, Baker, or ChemPur were used.

Crystallographic data were collected using an XtaLAB Synergy, Dualflex, HyPix diffractometer at $T = 100.00(10)$ K.

Routine UV spectra were recorded with a CINTRA 4040 spectrophotometer (GBC, Dandenong, Australia). UV-monitored melting experiments were performed at 260 nm in cuvettes with 1 cm path length using a UV-vis NIR spectrophotometer V-770 (Jasco, Japan) equipped with a 6 × 1 Peltier thermal cell.

For thermal dissociation experiments, oligonucleotide samples were dissolved in pH 7.2 buffer containing 10 mM Tris–HCl, 100 mM NaCl, and 10 mM $MgCl_2$. Annealing was performed from 85 °C to 15 °C with a temperature gradient of 1 °C min^{-1}. Melting profiles were recorded over a range of 15 → 85 °C (0.5 °C min^{-1}). Melting temperatures (T_m) were calculated using the software provided by Jasco.

P-Stereodefined PSCh oligonucleotides were synthesized manually at a 1 μmol scale, using the slightly modified previously published protocols.[16,35] The first nucleoside unit was anchored to the solid support by a DBU-resistant sarcosinyl–succinoyl linker [–C(O)CH$_2$CH$_2$C(O)–N(CH$_3$)CH$_2$C(O)–LCAA-CPG].[36] Routine coupling steps were performed using 20 mg of the dN-OTP monomers **1**. In the cycles where the monomers **2** or **3** were incorporated, double coupling was executed (20 mg + 20 mg) and in both steps the coupling time was extended to 20 minutes. The assembled DMT-labeled oligomers were cleaved from the support (25% NH_4OH, r.t., 3 h) and the protecting groups from nucleobases were removed with 25% NH_4OH_{aq} over 18 h ([PS]-{DNA:^{M}RNA}, 55 °C; [PS]-{DNA:^{T}RNA}, 37 °C). The samples were concentrated under reduced pressure and the DMT-labeled oligonucleotides were isolated using RP-HPLC. The collected fractions were concentrated under reduced pressure. The [PS]-{DNA:^{M}RNA} oligomers were detritylated with 50% $AcOH_{aq}$ for 20 minutes and the volatile components were evaporated. The TBDMS and DMT groups in [PS]-{DNA:^{T}RNA} oligomers were simultaneously removed by treatment with 3HF × NEt_3 at room temperature for 20 hours. The reagent was quenched with sterile water and all chimeric [PS]-oligomers were isolated by means of RP-HPLC. The identity of oligonucleotides was confirmed by MALDI-TOF MS (for the relevant spectra see ESI†).

Unmodified DNA and (2′-OMe)-RNA oligonucleotide matrices (**Md** and **Mm**, respectively) were synthesized on a Gene-World synthesizer (K&A Laborgeraete GbR, Schaafheim,

Germany) and routinely isolated by a two-step RP-HPLC method.

Synthesis of oxathiaphospholane monomers 2 and 3 – a general procedure

Oxathiaphospholane monomers **2** and **3** were synthesized analogously to a general procedure published for the synthesis of standard OTP monomers.[34] Briefly, a suitable nucleoside **4** (2 mmol, N-protected if necessary; Scheme 1) was dried overnight in a 25 mL round bottom flask with two necks (with a magnetic stirrer inside) at high vacuum (0.01 mm Hg). To the flask purged with dry argon, 10 mL of anhydrous pyridine was added using a gas-tight syringe. To the stirred solution, 0.36 mL of 2-chloro-4,4-pentamethylene-1,3,2-oxathiaphospholane (OTP-Cl, 0.51 g, 2.4 mmol) was added at room temperature for 5 minutes using a gas-tight syringe. After approximately 5 minutes, 0.2 g of dry elemental sulfur (approximately 6 mmol) was added, and stirring was continued at room temperature for 12 hours. Excess sulfur was filtered off, the solvent evaporated, and the residue dissolved in 2 mL of acid-free chloroform (distilled with pyridine). The crude product was applied to a silica gel column (glass tube 15 × 3 cm, height of gel suspension layer – 5 cm, 230–400 mesh) and the column was eluted with acid-free chloroform. Appropriate fractions (8–10 mL each, analyzed by TLC on silica gel 60 plates, Rf's are given in Table 1) were combined, and the solvent was evaporated under reduced pressure (15–20 mm Hg) at a water bath temperature not exceeding 30 °C. Anhydrous toluene (5–6 mL) was then added and the solution was evaporated to dryness excluding moisture. Finally, the samples were dried under high vacuum (oil pump) for 12 hours and stored at −15 °C. The yields of the isolated mixtures of P-diastereomers are given in Tables 1 and 2.

Detritylation of the *fast*-eluting diastereomer of 3a

To a solution of 120 mg (0.12 mmol) of *fast*-eluting isomer of 5′-*O*-DMT-2′-*O*-TBDMS-N^6-Bz-adenosine-3′-*O*-(2-thio-4,4-pentamethylene-1,3,2-oxathiaphospholane) in 2 mL of anhydrous acetonitrile a sodium hydrogen sulfate/silica gel reagent (50 mg) was added and the suspension was stirred at room temperature. The reaction progress was monitored by TLC using a 9 : 1 (v/v) chloroform : methanol mixture as an eluent (Rf of the substrate 0.57; Rf of the product 0.31). After 26 hours the reaction went to complete. The silica gel was filtered off and the solvent was evaporated *in vacuo*. The product was isolated by semipreparative HPLC (a silica gel column eluted with ethyl acetate) and evaporation at reduced pressure furnished white solid material (52 mg, 62%).

Details of X-ray data collection and reduction

Single colorless transparent plate-shaped crystals of the detritylated *fast*-eluting P-diastereomer of **3a** were obtained by recrystallization from a mixture of ethyl acetate and methanol (4 : 1 v/v). A suitable crystal of 0.11 × 0.08 × 0.02 mm dimension was selected and mounted on a suitable support. During data collection the crystal was kept at a steady temperature $T =$ 100.00(10) K. The structure was solved with the *XT* structure solution program[37] using an intrinsic phasing solution method and *Olex2* (ref. 38) as a graphical interface. The model was refined with *ShelXL* (version 2018/3; ref. 39), using the least squares minimization.

In solution synthesis of dinucleoside 3′,5′-phosphorothioates $^{M}N_{PS}T$ (8a) and $N_{PS}T$ (8b)

To a sample of a P-diastereomerically pure (*fast*- or *slow*-eluting) oxathiaphospholane monomer **2** or **3** (5 mg, *ca.* 5 μmol) and 3′-*O*-Ac-thymidine (3 mg, *ca.* 11 μmol), 600 μL of dry acetonitrile and 5 μL of 1,8-diazabicyclo-[5.4.0]undec-7-ene (DBU, 1.1 molar equivalent over the OTP monomers) were added under dry argon. After 2 h the reaction was complete. The acetonitrile was removed under reduced pressure and the products **6** were treated (in a tightly closed vessel) with concentrated ammonia solution (1 mL) for 18 h either at 55 °C (**6a**) or at 37 °C (**6b**), except for B = Ura (2 h at room temperature). The products **7a** were routinely detritylated using 50% $AcOH_{aq}$. In case of **7b**, approximately 10% of the ammoniacal solution was evaporated to dryness and the DMT and TBDMS moieties were removed with $3HFxNEt_3$ (150 μL, 17 h, room temperature) followed by evaporation under reduced pressure. The dimers **8** were isolated using RP-HPLC. Conditions: a C18 column, 250 × 4.6 mm, 5 μm; elution at 1.0 mL min^{-1} with a gradient of 0.1 M TEAB, pH 7.3 to 40% CH_3CN in 0.1 M TEAB over 20 minutes.

Conflicts of interest

There are no conflicts to declare.

Acknowledgements

This work was financially supported by National Centre of Science, Poland, grants UMO-2015/19/B/ST5/03116 (to P. G.) and UMO-2021/43/D/ST4/02433 (to K. J.). An Avance Neo 400 NMR spectrometer was purchased using funds provided by the EU Regional Operational Program of the Lodz Region, RPLD.01.01.00-10-0008/18.

Notes and references

1 F. Eckstein, *Angew. Chem., Int. Ed. Engl.*, 1983, **22**, 423; W. J. Stec, G. Zon, W. Egan and B. Stec, *J. Am. C. Soc.*, 1984, **106**, 6077; F. Eckstein, *Annu. Rev. Biochem.*, 1985, **54**, 367; F. Eckstein, *Antisense Nucleic Acid Drug Dev.*, 2000, **10**, 117.
2 C. A. Stein, *Biochim. Biophys. Acta*, 1999, **1489**, 45.
3 A. M. Krieg, *Antisense Nucleic Acid Drug Dev.*, 2001, **11**, 181.
4 A. M. Krieg, P. Guga and W. J. Stec, *Oligonucleotides*, 2003, **13**, 491.
5 S. T. Crooke, S. Wang, T. A. Vickers, W. Shen and X. Liang, *Nat. Biotechnol.*, 2017, **35**, 230.
6 Q. Laurent, R. Martinent, D. Moreau, N. Winssinger, N. Sakai and S. Matile, *Angew. Chem., Int. Ed.*, 2021, **60**, 19102.

7 S. T. Crooke, P. P. Seth, T. A. Vickers and X. Liang, *J. Am. Chem. Soc.*, 2020, **142**, 14754.
8 L. Wang, S. Chen S, T. Xu, K. Taghizadeh, J. S. Wishnok, X. Zhou, D. You, Z. Deng and P. C. Dedon, *Nat. Chem. Biol.*, 2007, **3**, 709.
9 L. Xiong, S. Liu, S. Chen, Y. Xiao, B. Zhu, Y. Gao, Y. Zhang, B. Chen, J. Luo, Z. Deng, X. Chen, L. Wang and S. Chen, *Nat. Commun.*, 2019, **10**, 1.
10 P. Guga and M. Koziołkiewicz, *Chem. Biodiversity*, 2011, **8**, 1642.
11 Y. Wu, Y. Tang, X. Dong, Y. Y. Zheng, P. Haruehanroengra, S. Mao, Q. Lin and J. Sheng, *ACS Chem. Biol.*, 2020, **15**, 1301.
12 P. A. Frey and R. D. Sammons, *Science*, 1985, **228**, 541.
13 W. J. Stec, A. Grajkowski, M. Koziołkiewicz and B. Uznański, *Nucleic Acids Res.*, 1991, **19**, 5883.
14 A. Wilk, A. Grajkowski, L. R. Phillips and S. L. Beaucage, *J. Am. Chem. Soc.*, 2000, **122**, 2149.
15 N. Oka, M. Yamamoto, T. Sato and T. Wada, *J. Am. Chem. Soc.*, 2008, **130**, 16031.
16 W. J. Stec, B. Karwowski, M. Boczkowska, P. Guga, M. Koziołkiewicz, M. Sochacki, M. Wieczorek and J. Błaszczyk, *J. Am. Chem. Soc.*, 1998, **120**, 7156.
17 M. Boczkowska, P. Guga and W. J. Stec, *J. Biomol. Struct. Dyn.*, 1999, **16**, 1291.
18 T. Inagawa, H. Nakashima, B. Karwowski, P. Guga, W. J. Stec, H. Takeuchi and H. Takaku, *FEBS Lett.*, 2002, **528**, 48.
19 P. Guga, *Curr. Top. Med. Chem.*, 2007, **7**, 695.
20 P. Guga, M. Boczkowska, M. Janicka, A. Maciaszek, S. Kuberski and W. J. Stec, *Biophys. J.*, 2007, **92**, 2507.
21 P. Guga, M. Janicka, A. Maciaszek, B. Rębowska and G. Nowak, *Biophys. J.*, 2007, **93**, 3567.
22 P. Guga, A. Maciaszek and W. J. Stec, *Org. Lett.*, 2005, **7**, 3901.
23 A. Sierzchała, A. Okruszek and W. J. Stec, *J. Org. Chem.*, 1996, **61**, 6713.
24 N. Oka, T. Kondo, S. Fujiwara, Y. Maizuru and T. Wada, *Org. Lett.*, 2009, **11**, 967.
25 Y. Nukaga, K. Yamada, T. Ogata, N. Oka and T. Wada, *J. Org. Chem.*, 2012, **77**, 7913.
26 W. J. Stec, A. Grajkowski, A. Kobylańska, B. Karwowski, M. Koziołkiewicz, K. Misiura, A. Okruszek, A. Wilk, P. Guga and M. Boczkowska, *J. Am. Chem. Soc.*, 1995, **117**, 12019.
27 K. Jastrzębska, A. Maciaszek, R. Dolot, G. Bujacz and P. Guga, *Org. Biomol. Chem.*, 2015, **13**, 10032.
28 A. Tomaszewska-Antczak, K. Jastrzębska, A. Maciaszek, B. Mikołajczyk and P. Guga, *RSC Adv.*, 2018, **8**, 24942.
29 E. Radzikowska, R. Kaczmarek, D. Korczyński, A. Krakowiak, B. Mikołajczyk, J. Baraniak, P. Guga, K. A. Wheeler, T. Pawlak and B. Nawrot, *RSC Adv.*, 2020, **10**, 35185.
30 R. Wallin, M. Kalek, A. Bartoszewicz, M. Thelin and J. Stawinski, *Phosphorus, Sulfur, and Silicon*, 2009, **184**, 908; N. Wang, P. Saidhareddy and X. Jiang, *Nat. Prod. Rep.*, 2020, **37**, 246.
31 R. K. Kannasani, V. V. S. Peruri and S. R. Battula, *Chem. Cent. J.*, 2012, **6**, 136.
32 L. J. Farrugia, *J. Appl. Crystallogr.*, 2012, **45**, 849.
33 H. Kaur, J. Wengel and S. Maiti, *Biochemistry*, 2008, **47**, 1218–1227.
34 R. Dolot, A. Maciaszek, B. Mikołajczyk and B. Nawrot, *Crystals*, 2022, **12**, 760.
35 P. Guga and W. J. Stec, in *Current Protocols in Nucleic Acid Chemistry*, ed. S. L. Beaucage, D. E. Bergstrom, G. D. Glick and R. A. Jones, John Wiley and Sons, Hoboken, N. J., 2003, p. 4.17.1.
36 T. Brown, C. E. Pritchard, G. Turner and S. A. Salisbury, *J. Chem. Soc., Chem. Commun.*, 1989, 891.
37 G. M. Sheldrick, *Acta Crystallogr., Sect. A: Found. Adv.*, 2015, **71**, 3.
38 L. J. Bourhis, O. V. Dolomanov, R. J. Gildea, J. A. K. Howard and H. Puschmann, *Acta Crystallogr., Sect. A: Found. Adv.*, 2015, **71**, 59.
39 G. M. Sheldrick, *Acta Crystallogr., Sect. C: Struct. Chem.*, 2015, **71**, 3.